TOMOGRAPHY® RESEARCH ARTICLE

Quantitative Comparison of Prone and Supine PERCIST Measurements in Breast Cancer

Jennifer G. Whisenant[1,2], Jason M. Williams[3], Hakmook Kang[3,4], Lori R. Arlinghaus[3], Richard G. Abramson[1,3,5], Vandana G. Abramson[1,2], Kareem Fakhoury[6], A. Bapsi Chakravarthy[1,7], and Thomas E. Yankeelov[8]

[1]Vanderbilt-Ingram Cancer Center, Vanderbilt University Medical Center, Nashville, TN; [2]Department of Medicine, Vanderbilt University Medical Center, Nashville, TN; [3]Vanderbilt University Institute of Imaging Science, Vanderbilt University Medical Center, Nashville, TN; [4]Department of Biostatistics, Vanderbilt University Medical Center, Nashville, TN; [5]Department of Radiology and Radiological Sciences, Vanderbilt University Medical Center, Nashville, TN; [6]Department of Radiation Oncology, University of Colorado Cancer Center—Anschutz Medical Campus, Aurora, CO; [7]Department of Radiation Oncology, Vanderbilt University Medical Center, Nashville, TN; and [8]Oden Institute for Computational Engineering and Sciences; Livestrong Cancer Institutes; Department of Biomedical Engineering; Department of Diagnostic Medicine; and Department of Oncology, The University of Texas, Austin, TX

Corresponding Author:
Jennifer G. Whisenant, PhD
Department of Medicine, Vanderbilt University Medical Center, 2220 Pierce Avenue, 691 PRB, Nashville, TN 37209;
E-mail: j.whisenant@vumc.org

Key Words: FDG-PET, pathological complete response, quantitative PET, 18F-fluorodeoxyglucose

Abbreviations: area under the curve (AUC), confidence interval (CI), 18F-fluorodeoxyglucose (FDG), false discovery rate (FDR), human epidermal receptor 2 (HER2), magnetic resonance imaging (MRI), metabolic tumor volume (MTV), neoadjuvant therapy (NAT), positron emission tomography (PET), receiver operating characteristic (ROC), standardized uptake value (SUV), SUV normalized to lean muscle (SUL), volume of interest (VOI)

ABSTRACT

Positron emission tomography (PET) is typically performed in the supine position. However, breast magnetic resonance imaging (MRI) is performed in prone, as this improves visibility of deep breast tissues. With the emergence of hybrid scanners that integrate molecular information from PET and functional information from MRI, it is of great interest to determine if the prognostic utility of prone PET is equivalent to supine. We compared PERCIST (PET Response Criteria in Solid Tumors) measurements between prone and supine FDG-PET in patients with breast cancer and the effect of orientation on predicting pathologic complete response (pCR). In total, 47 patients were enrolled and received up to 6 cycles of neoadjuvant therapy. Prone and supine FDG-PET were performed at baseline (t_0; n = 46), after cycle 1 (t_1; n = 1) or 2 (t_2; n = 10), or after all neoadjuvant therapy (t_3; n = 19). FDG uptake was quantified by maximum and peak standardized uptake value (*SUV*) with and without normalization to lean body mass; that is, SUV_{max}, SUV_{peak}, SUL_{max}, and SUL_{peak}. PERCIST measurements were performed for each paired baseline and post-treatment scan. Receiver operating characteristic analysis for the prediction of pCR was performed using logistic regression that included age and tumor size as covariates. *SUV* and *SUL* metrics were significantly different between orientation ($P < .001$), but were highly correlated ($P > .98$). Importantly, no differences were observed with the PERCIST measurements ($P > .6$). Overlapping 95% confidence intervals for the receiver operating characteristic analysis suggested no difference at predicting pCR. Therefore, prone and supine PERCIST in this data set were not statistically different.

INTRODUCTION

Historically, patients with locally advanced breast cancer were treated with radical surgery followed by adjuvant chemotherapy. Today, neoadjuvant therapy (NAT) is used to downstage tumors in order to allow for breast conservation, convert patients from inoperable to operable, and provide an in vivo marker of tumor response for the individual patient (1–5). Histopathology obtained from surgical specimens serves as the reference standard for evaluating response to NAT, and the documentation of a pathological complete response (pCR) in the breast and axillary tissue at the time of definitive surgery is associated with long-term survival (6–8). Thus, methods that can predict therapeutic efficacy at an early time point could help to individualize treatment and potentially avoid ineffective therapies.

The introduction of molecularly targeted therapies has underscored a critical need to develop and validate highly specific and robust biomarkers to assay the clinical and biological activity of these interventions. Positron emission tomography (PET) is recognized as an imaging technique that can provide a molecular and physiological assessment of a specific tissue. PET with the glucose analog ^{18}F-fluorodeoxyglucose (FDG) is the most frequently used radiotracer in oncology. To assess treatment response with FDG-

ISSN 2379-1381 https://doi.org/10.18383/j.tom.2020.00002

Table 1. Patient and Tumor Characteristics (N = 47)

Median Age, Years (Range)	48 (31–67)	
Race and Ethnicity	N	%
White	35	74%
Black or African American	12	26%
Hispanic or Latino	2	4%
Clinical Stage	N	%
I	5	11%
IIA	10	21%
IIB	13	28%
IIIA	14	30%
IIIB	2	4%
IIIC	2	4%
IV	1	2%
Median Tumor Diameter at Baseline, cm (Range)	5 (1–13)	
Receptor Status	N	%
Hormone Receptor–Positive, HER2-Positive	8	17%
Hormone Receptor–Positive, HER2-Negative	10	21%
Hormone Receptor–Negative, HER2-Positive	12	26%
Hormone Receptor–Negative, HER2-Negative (Triple Negative)	17	36%
Tumor Response	N	%
pCR	26	55%
Non-pCR	18	38%
No Surgery	3	6%

Abbreviations: HER2: human epidermal receptor 2; pCR: pathologic complete response.

PET, Wahl et al. (9) developed the PET Evaluation Response Criteria in Solid Tumors (PERCIST), which quantifies the percent change from baseline in radiotracer uptake after therapy. Guidelines based on thresholds of percent change in FDG uptake provide definitions of tumor response and disease progression as a function of metabolic activity.

For breast imaging, FDG-PET is traditionally performed with the patient in the supine position with arms over the head. However, several studies have suggested that scanning with the patient in the prone position is superior for breast imaging as it provides improved separation of deep breast and axillary tissue from the chest wall (10–12). Furthermore, the introduction of hybrid PET/magnetic resonance imaging (MRI) systems provide additional motivation for studying prone FDG-PET, as breast MRI is performed in the prone position. There are 2 issues of relevance in comparing prone versus supine, first is the issue of sensitivity and specificity of lesion detectability, and the second is with regard to quantification of radiotracer uptake in the tumor. We have previously published on the former question, and showed improved visibility of cancer-involved lymph nodes, and thus a potential improvement in diagnostic assessment when FDG-PET of the breast was performed in the prone position (13). The scope of the current work addresses the second issue; in particular, the main objective was to compare PERCIST measurements calculated from prone and supine data in patients with breast cancer who underwent longitudinal FDG-PET during NAT. As a secondary objective, the ability to predict pCR was compared between prone and supine FDG-PET.

METHODOLOGY

Patients

As part of a prospective longitudinal imaging study [NCT01222416; see (13–15)], eligible subjects were those diagnosed with measurable, histologically proven breast cancer and scheduled to undergo NAT. FDG-PET/CT was performed at 3 of the following 4 potential time points: before the start of NAT (t_0), after the first cycle of therapy (t_1), and either after the second treatment cycle (t_2) or after completion of all cycles (t_3). For patients who went on to surgery, pathologic response (pCR or non-pCR) was recorded for each patient. This protocol was approved by the Institutional Review Board of Vanderbilt University Medical Center. All study procedures were performed in accordance with the World Association Declaration of Helsinki Ethical Principles for Medical Research involving human subjects, and all study participants provided written informed consent to join the study.

Preparation

Patients fasted at least 6 hours before each imaging session. Before each scan, serum glucose was assayed and verified to be $<$200 mg/dL. Approximately 258.9 MBq/kg of FDG (median, 254.5 MBq/kg; range, 191.4–334.4) was delivered into the antecubital vein contralateral to the affected breast. After injection, patients remained inactive in a dimmed room for ~60 minutes; after this uptake period, patients voided the bladder and were positioned onto the imaging table.

Data Acquisition

Images were collected using a Discovery STE clinical PET scanner (GE Healthcare, Waukesha, WI) with arms raised above the head. Data were acquired in the following 2 orientations: in the prone position using a custom-built padded support device (13, 16) and in the standard supine position without the device. Both protocols featured 3D acquisition with 47 slices per bed position with an 11-slice overlap between bed positions: for the prone scan, 94 slices over 2 bed positions were acquired (ie, 83 contiguous slices from the bottom of the skull to mid-abdomen); for the supine scan, 376 slices over 8 bed positions were acquired (ie, 299 contiguous slices from the top of the skull to mid-thigh). For all but 2 subjects, data were first collected with the subject in the prone orientation, followed by supine orientation. PET images were reconstructed iteratively (20 subsets, 2 iterations, 6-mm smoothing), resulting in a 3.27-mm slice thickness and a 128 × 128 axial field-of-view matrix (5.47-mm^2 pixel size). Each PET scan was accompanied by a low-milliampere CT without contrast to correct for attenuation artifacts and provide anatomic localization.

Volume-of-Interest Analysis. Using standard methods (17, 18), in-house algorithms were written in MATLAB (MathWorks, Natick, MA) to convert raw pixel intensity data from each

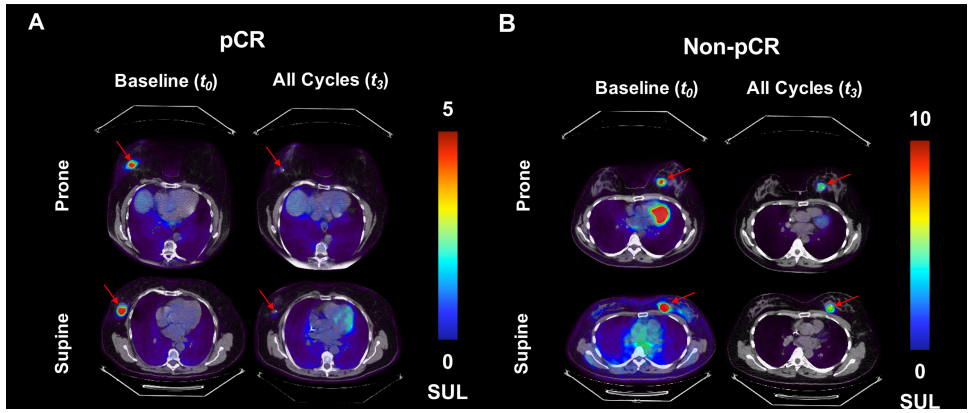

Figure 1. Representative examples of prone and supine 18F-fluorodeoxyglucose (FDG) positron emission tomography (PET)/computed tomography (CT) images for a patient with pathologic complete response (pCR) ["responder"; (A)] and a patient with non-pCR patient ["nonresponder"; (B)] are presented at baseline and after all cycles of neoadjuvant therapy. The image corresponding to the central tumor slice is presented for each subject. FDG uptake decreased in both patients after therapy, although the responder had the largest decrease in radiotracer accumulation. In addition, the spatial distribution of radiotracer uptake within the lesion appears to be larger in the supine position than in the prone position, especially visible in the nonresponder (B). Also noted in (B) is the radiotracer accumulation within the myocardium of the heart in the prone images at baseline. Similar uptake is observed within the myocardium in the supine image at baseline, as well as both prone and supine image post-treatment. However the images that included the central tumor slice did not include the same anatomical section of the heart.

DICOM series into standardized uptake values (*SUV*) as previously described (15, 16). The *SUV* normalized to lean muscle (*SUL*) was calculated as $\frac{A}{(I'/LBM)}$, where A is the activity concentration (Bq/mL) in the PET image, I' is the decay-corrected injected activity (Bq), and *LBM* is the patient's lean body mass (g) (9). PET/CT image fusion and visualization was carried out using OsiriX (Pixmeo, Geneva, Switzerland). Volumes of interest (VOIs) were manually drawn over contiguous axial *SUL* images that encompassed the breast lesion. Four metrics from these VOIs were calculated at each imaging time point: the maximum single-voxel *SUV* (SUV_{max}) and *SUL* (SUL_{max}) and the mean value of a 1-cm^3 sphere (SUV_{peak}, SUL_{peak}), also known as the "hotspot"\ analysis (9). For each metric, PERCIST measurements (or percent change) were performed for each baseline image that had at least 1 corresponding post-baseline scan by using the following formula from Wahl et al. (9):

$$\%\,\text{Change} = \frac{100 \times (t_n - t_0)}{t_0},$$

where t_0 and t_n are the baseline and post-baseline scans, respectively. For simplicity, we are defining "PERCIST measurement" to be the percent change equation (listed) above. We note that PERCIST is a series of guidelines that quantify tumor uptake and compute percent change to evaluate tumor response based on thresholds of change. The interested reader should refer to the literature (9, 19) for more detail regarding PERCIST guidelines.

Statistical Analyses

To compare the difference between prone and supine, a Wilcoxon signed rank test was performed for each metric, including the PERCIST measurement. A Spearman correlation was performed to test for association between scan orientations for each metric. A Bland–Altman analysis (20) was performed to test for agreement between scan orientations. Lastly, a receiver operating characteristic (ROC) curve analysis was performed to determine the ability of each measurement (ie percent change of each imaging metric; for example, SUL_{peak}) to predict pCR using a logistic regression model that included age and tumor size as covariates; areas under the ROC curve (AUC) were subsequently calculated. P values of $\leq$0.05 were considered statistically significant. Correction for multiple testing was performed by controlling the FDR (false discovery rate) at 0.05.

RESULTS

Patient Characteristics and Pathologic Response

In total, 47 treatment-naïve patients with breast cancer were enrolled. Patients received up to 6 cycles of NAT (regimens listed in online supplemental Table 1 for each patient) followed by surgery if appropriate. Patient baseline characteristics and pathologic response are listed in Table 1. Median age was 48 years (range, 31–67). Patients with a range of clinical stages were included, with the majority being stage IIIA (30%), followed closely by IIB (28%) and IIA (21%). The median tumor size was 5.0 cm (range, 1–13). In addition, a range of receptor statuses were observed: 36% were hormone receptor and human epidermal receptor 2 (HER2)–negative (triple negative), 26% were hormone receptor–negative but positive for HER2, 21% were hormone receptor–positive but HER2-negative, and 17% were both hormone receptor–positive and HER2-positive. After NAT, 18 (38%) patients achieved pCR (ie responders), while 26 (55%)

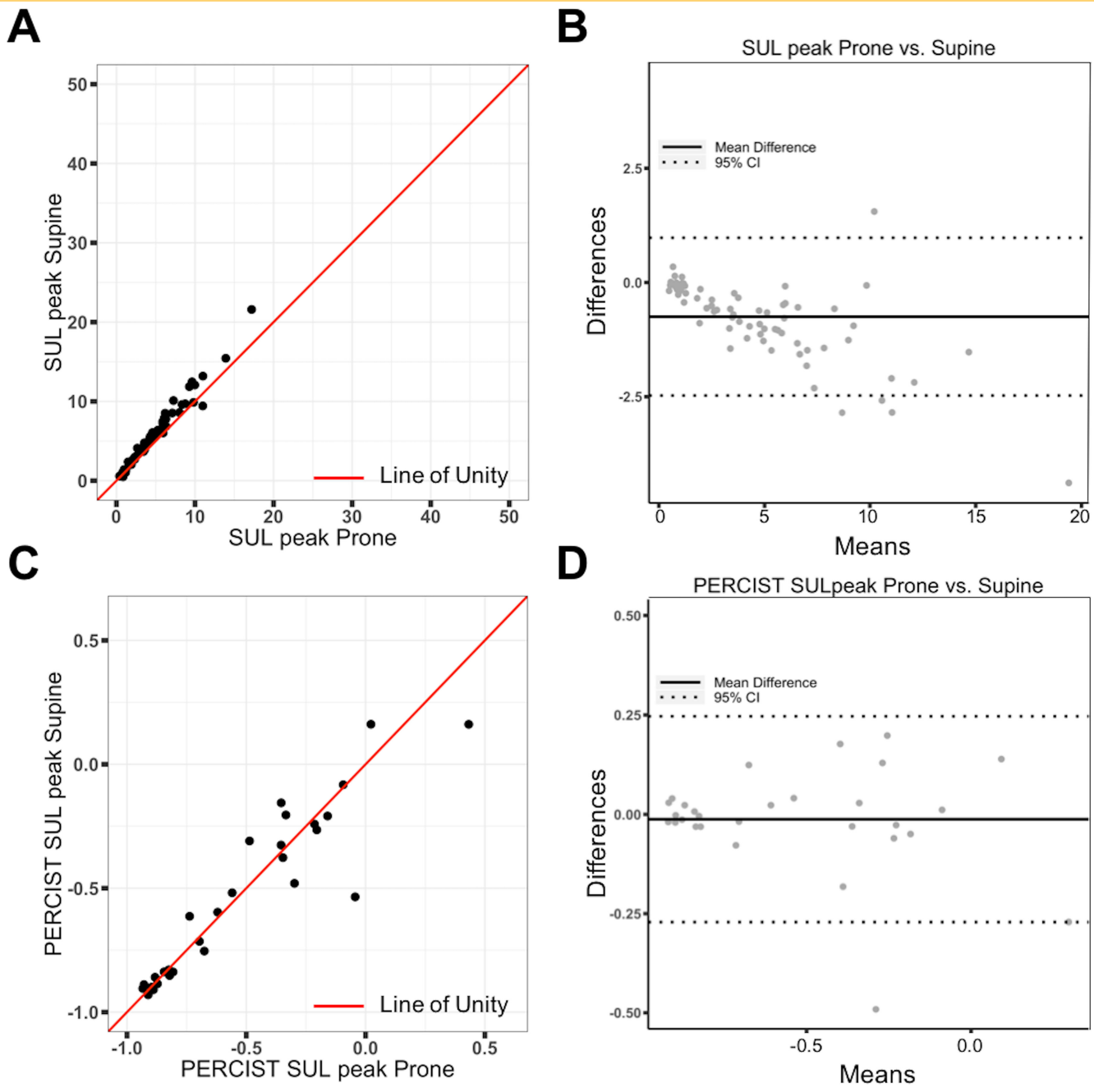

Figure 2. Scatter plot of standardized uptake value (SUV) normalized to lean muscle (SUL_{peak}) from supine images plotted against SUL_{peak} from prone images (A). This plot shows that although the supine values are statistically higher than the prone values, values from the 2 scans are consistent. Line of unity is shown as the red solid line. Bland–Altman plot again shows that the SUL_{peak} from supine and prone data is consistent and is in good agreement as most data points are within the 95% confidence interval limits (B). Scatter and Bland–Altman plots for the PERCIST (PET Response Criteria in Solid Tumors) measurement of SUL_{peak} (C, D). The line of unity is located within the middle of the data points, suggesting the PERCIST values are similar in value. The Bland–Altman plot again shows good agreement between prone and supine data. Please note the difference in scales on the *y* axis of the Bland–Altman plots in (B) and (D). Notably, the width of the 95% confidence intervals are smaller with the PERCIST measurement compared to the absolute metrics.

did not (ie nonresponders). Three patients did not undergo surgery; 1 was diagnosed on initial PET scan as having widespread metastatic disease, and the other 2 developed metastatic disease in the brain while undergoing NAT.

Owing to a variety of factors, not all patients were scanned at all time points. Therefore, the number of FDG-PET/CT prone and supine scans at each time point is as follows: baseline (t_0; n = 46), after cycle 1 (t_1; n = 2), after cycle 2 (t_2; n = 10), or after

Table 2. PET/CT Parameter Comparison: Prone Versus Supine

	Mean Prone (±SD)	Mean Supine (±SD)	Mean difference (±SD)	Wilcoxon Test	Spearman Correlation (*p* value)
Absolute Metrics					
SUV_{max}	8.21 (±6.97)	9.78 (±8.54)	−1.57 (±2.08)	$P < .001$	0.985 (<0.001)
SUV_{peak}	6.68 (±5.81)	7.95 (±7.03)	−1.27 (±1.54)	$P < .001$	0.991 (<0.001)
SUL_{max}	5.15 (±4.16)	6.11 (±5.01)	−0.96 (±1.23)	$P < .001$	0.986 (<0.001)
SUL_{peak}	4.19 (±3.49)	4.96 (±4.16)	−0.78 (±0.91)	$P < .001$	0.989 (<0.001)
PERCIST Measurements					
SUV_{max}	−0.53 (±0.34)	−0.54 (±0.34)	0.00 (±0.13)	$P = .639$	0.911 (<0.001)
SUV_{peak}	−0.52 (±0.36)	−0.53 (±0.34)	0.02 (±0.13)	$P = .848$	0.931 (<0.001)
SUL_{max}	−0.54 (±0.34)	−0.54 (±0.33)	0.00 (±0.13)	$P = .609$	0.916 (<0.001)
SUL_{peak}	−0.52 (±0.36)	−0.54 (±0.33)	0.02 (±0.13)	$P = .831$	0.930 (<0.001)

SD: standard deviation; means include all time points with corresponding prone and supine data; mean difference is prone − supine.

all NAT (t_3; n = 19). Factors resulting in a loss of imaging data at these time points included changes in the course of therapy due to disease progression and patients declining follow-up scanning due to scheduling conflicts or feeling too ill.

PET/CT Parameter Comparison and Pathologic Response

Illustrative FDG-PET/CT images are presented in Figure 1 for a subject with pCR (ie responder) and for another without pCR (ie nonresponder). The image corresponding to the central tumor slice is presented for each subject. As expected, the breast lesion, and subsequently the tumor FDG uptake, disappeared for the responder (Figure 1A), whereas the breast lesion and FDG uptake was still observed after NAT for the nonresponder (Figure 1B). FDG-PET/CT metrics at each time point are listed for each subject in online supplemental Table 2.

Scatter plots for the value of each metric were graphed, and an illustrative example of SUL_{peak} from supine images plotted against SUL_{peak} from prone images is shown in Figure 2A; the line of unity (red line) is also presented. Notably, the supine values are significantly ($P = .001$) higher than the prone values; however, the 2 values are correlated (Table 2). A Bland–Altman plot (Figure 2B) also demonstrated that the SUL_{peak} from supine and prone data is consistent and in good agreement as most data points are within the 95% confidence interval limits. Scatter and Bland–Altman plots for the PERCIST measurement of SUL_{peak} show no statistical difference between prone and supine orientation (Figure 2, C and D); similar results were observed for the other PERCIST measurements (Table 2). Scatter and Bland–Altman plots for all other metrics are included in online supplemental Figures 1–3.

In total, 29 PERCIST measurements were computed for each scanning position and PET metric, 10 after cycle 2 and 19 after all cycles of NAT; this corresponded to PET data for 28 patients, as scans were performed at 3 time points for 1 patient. Age and tumor size along with each PERCIST measurement were included as covariates in a logistic regression model for prediction of pCR. AUC values (±95% confidence intervals) were calculated to compare the ability of prone versus supine measurements to predict response, and are listed in Table 3. The AUC values for the prone metrics ranged between 0.73 and 0.75, which were slightly lower than the supine metrics that ranged between 0.77 and 0.79. However, the 95% confidence intervals for each imaging metric overlap, suggesting no difference between scan position at predicting pCR.

DISCUSSION

Breast MRI is recommended for evaluation of disease extent in patients with biopsy-proven breast cancer just before surgery, and the utility of this modality to predict response to NAT is an active area of investigation (21–26). By combining the molecular information of PET with the morphological and functional information provided by MRI, it is possible to provide a more comprehensive biological assessment of a lesion. Breast MRI is collected in the prone position to minimize patient motion and reduce image contamination from other organs such as the heart. Traditionally, however, PET is collected in the supine position, making a direct voxel-by-voxel comparison with MRI very challenging. With the development of combined PET/MRI systems, PET data can now be collected in the prone position similar to MRI. When comparing prone versus supine information, there are the following 2 relevant issues: lesion detectability and lesion quantification. Regarding lesion detectability, we have previously shown that prone and supine FDG-PET provided statistically identical information regarding locoregional disease distribution in patients with breast cancer. Notably, we also showed improved lesion detectability of cancer-involved lymph nodes in the axilla of prone scans compared to supine (13), suggesting prone scans have improved diagnostic potential.

The focus of the current study was to compare radiotracer uptake, as quantified by PERCIST measurements, between prone and supine scans, as well as explore the effect, if any, on predicting pCR. It is known that the degree of compression and extension of tissue can affect an imaging measurement, which is why X-ray mammography uses compression to improve visualization of structures within the breast. It is plausible that the degree to

Table 3. PERCIST AUC Values with 95% Confidence Intervals (CI)

	Prone (95% CI)	Supine (95% CI)
SUV_{max}	0.74 (0.53–0.95)	0.77 (0.58–0.97)
SUV_{peak}	0.73 (0.52–0.94)	0.77 (0.57–0.97)
SUL_{max}	0.75 (0.55–0.96)	0.79 (0.60–0.98)
SUL_{peak}	0.74 (0.53–0.95)	0.78 (0.58–0.98)

Abbreviations: PERCIST, PET Evaluation Response Criteria in Solid Tumors; AUC, area under curve; SUV, standardized uptake value; SUL, standardized uptake value normalized to lean muscle.

which the breast is compressed or extended could also influence the local distribution of the radiotracer, which would then have an effect on the uptake within the breast tissue and thus the PERCIST measurement. Therefore, the main objective of this study was to determine if the different orientation of the breast during prone and supine PET imaging had a statistically significant effect on the resulting image quantification, namely, the PERCIST measurements, and the ability to predict pCR.

Results from this study suggest that PERCIST measurements, regardless of metric (eg, *SUV*, *SUL*) calculated from prone data are not statistically different to supine data. In addition, the ROC analysis showed no difference in predicting pCR between scan positions. This result is especially important given the increasing investigation of combined PET and MRI studies to provide complementary information of the breast tumor and its microenvironment (14, 27–29). Interestingly, a comparison of the individual PET metrics (eg, SUV_{max} or SUL_{max}) between scan positions showed that the supine values were significantly higher than the prone. In addition, a linear pattern is observed in the Bland–Altman plot (Figure 2B) where the difference between scan position increases as radiotracer uptake increases, suggesting the absolute metrics (*SUV*, *SUL*) are dependent on scan position. These results are consistent with our previous study that compared SUV_{peak} and SUV_{max} calculated from prone and supine FDG-PET in a breast phantom and patients with breast cancer (16). However, in both the current study and our previous work, the individual metrics were highly correlated between scan orientation and thus appeared to report on the same underlying pathophysiology. Notably, the proportional bias observed in the Bland–Altman plot was not observed in the PERCIST measurement comparison (Figure 2D).

Higher PET metrics calculated from the supine data could be due to a larger tissue per unit volume in the supine position, resulting in more positron emission counts from a particular tissue area of the breast. An example of this can be seen in Figure 1B where the lesion appears to be spatially broader with a larger footprint of "hotter" voxels in the supine orientation compared with prone orientation. Another potential reason as to why the supine PET metrics are higher than the prone PET metrics is the longer distribution time, and thus accumulation, of the radiotracer, thereby resulting in higher individual PET metrics. In all but 2 patients, the prone data were collected first. Notably, in the 2 patients where supine data were collected first, the prone metrics were higher (see online supplemental Table 2). Therefore, the significant difference in the individual metrics (SUV_{max} or SUL_{max}) is hypothesized to be an artifact of the study design. To completely remove the potential variable of acquisition time in relation to radiotracer administration, patients in this study should have been randomized to undergo either supine first or prone first. This represents a limitation, and a future study should randomize the sequence order of prone and supine data to explore if the individual PET metrics are truly different between scan orientations.

In conclusion, this study was performed to explore the difference in PERCIST measurements between prone and supine scan orientation in FDG-PET/CT of the breast. For all PET metrics (SUV_{peak}, SUV_{max}, SUL_{peak}, and SUL_{max}) evaluated, no statistical differences in PERCIST measurements were observed, suggesting that the orientation of the breast does not affect a PET measurement of percent change between 2 time points. This is of particular importance as the use of combined PET/MRI machines in the clinic increases and the utility of imaging biomarkers to provide a surrogate of pathological response becomes standard-of-care. Although this study was performed with FDG, it is anticipated that these results can be translated to another ^{18}F-labeled tracer and provide evidence that a corresponding PERCIST measurement collected in the prone position would be statistically not different than the supine.

Supplemental Materials

Supplemental Data: https://doi.org/10.18383/j.tom.2020.00002.sup.01

ACKNOWLEDGMENTS

We would like to thank the patients and their families for participating in this ancillary imaging study. We would also like to thank the NIH/NCI (U01 CA142565, 1U01 CA174706, P50 CA098131, P30 CA68485), CPRIT (RR160005; T.E.Y. is a CPRIT Scholar in Cancer Research), NIH/NCATS (UL1TR000445), and the Kleberg Foundation for supporting this study.

Conflict of Interest: None reported.

Disclosures: No disclosures to report.

REFERENCES

1. Tryfonidis K, Senkus E, Cardoso MJ, Cardoso F. Management of locally advanced breast cancer-perspectives and future directions. Nat Rev Clin Oncol. 2015;12:147–162.
2. Early Breast Cancer Trialists' Collaborative G. Long-term outcomes for neoadjuvant versus adjuvant chemotherapy in early breast cancer: meta-analysis of individual patient data from ten randomised trials. Lancet Oncol. 2018;19:27–39.
3. Mougalian SS, Soulos PR, Killelea BK, Lannin DR, Abu-Khalaf MM, DiGiovanna MP, Sanft TB, Pusztai L, Gross CP, Chagpar AB. Use of neoadjuvant chemotherapy for patients with stage I to III breast cancer in the United States. Cancer. 2015;121:2544–2552.
4. Clough KB, Acosta-Marin V, Nos C, Alran S, Rouanet P, Garbay JR, Giard S, Verhaeghe JL, Houvenaeghel G, Flipo B, Dauplat J, Dorangeon PH, Classe JM, Rouzier R, Bonnier P. Rates of neoadjuvant chemotherapy and oncoplastic surgery for breast cancer surgery: a French national survey. Ann Surg Oncol. 2015;22:3504–3511.
5. Vugts G, Maaskant-Braat AJ, Nieuwenhuijzen GA, Roumen RM, Luiten EJ, Voogd AC. Patterns of care in the administration of neo-adjuvant chemotherapy for breast cancer. A population-based study. Breast J. 2016;22:316–321.
6. Cortazar P, Zhang L, Untch M, Mehta K, Costantino JP, Wolmark N, Bonnefoi H, Cameron D, Gianni L, Valagussa P, Swain SM, Prowell T, Loibl S, Wickerham DL, Bogaerts J, Baselga J, Perou C, Blumenthal G, Blohmer J, Mamounas EP, Bergh J, Semiglazov V, Justice R, Eidtmann H, Paik S, Piccart M, Sridhara R, Fasching PA, Slaets L, Tang S, Gerber B, Geyer CE, Jr., Pazdur R, Ditsch N, z G. Pathological complete response and long-term clinical benefit in breast cancer: the CTNeoBC pooled analysis. Lancet. 2014;384:164–172.
7. Feldman LD, Hortobagyi GN, Buzdar AU, Ames FC, Blumenschein GR. Pathological assessment of response to induction chemotherapy in breast cancer. Cancer Res. 1986;46:2578–2581.
8. von Minckwitz G, Untch M, Blohmer JU, Costa SD, Eidtmann H, Fasching PA, Gerber B, Eiermann W, Hilfrich J, Huober J, Jackisch C, Kaufmann M, Konecny GE, Denkert C, Nekljudova V, Mehta K, Loibl S. Definition and impact of pathologic complete response on prognosis after neoadjuvant chemotherapy in various intrinsic breast cancer subtypes. J Clin Oncol. 2012;30:1796–1804.
9. Wahl RL, Jacene H, Kasamon Y, Lodge MA. From RECIST to PERCIST: evolving considerations for PET response criteria in solid tumors. J Nucl Med. 2009;50:122S–150S. doi:50/Suppl_1/122S [pii] 10.2967/jnumed.108.057307
10. Teixeira SC, Koolen BB, Vogel WV, Wesseling J, Stokkel MPM, Vrancken Peeters M-JTFD, van der Noort V, Rutgers EJT, Valdés Olmos RA. Additional prone 18F-FDG PET/CT acquisition to improve the visualization of the primary tumor and regional lymph node metastases in stage II/III breast cancer. Clin Nucl Med. 2016;41:e181–186.
11. Yutani K, Tatsumi M, Uehara T, Nishimura T. Effect of patients being prone during FDG PET for the diagnosis of breast cancer. AJR Am J Roentgenol. 1999;173:1337–1339.
12. Khalkhali I, Mena I, Diggles L. Review of imaging techniques for the diagnosis of breast cancer: a new role of prone scintimammography using technetium-99m sestamibi. Eur J Nucl Med. 1994;21:357–362.
13. Abramson RG, Lambert KF, Jones-Jackson LB, Arlinghaus LR, Williams J, Abramson VG, Chakravarthy AB, Yankeelov TE. Prone versus supine breast FDG-PET/CT for assessing locoregional disease distribution in locally advanced breast cancer. Acad Radiol. 2015;22:853–859.
14. Atuegwu NC, Li X, Arlinghaus LR, Abramson RG, Williams JM, Chakravarthy AB, Abramson VG, Yankeelov TE. Longitudinal, intermodality registration of quantitative breast PET and MRI data acquired before and during neoadjuvant chemotherapy: preliminary results. Med Phys. 2014;41:052302.
15. Williams JM, Arlinghaus LR, Rani SD, Shone MD, Abramson VG, Pendyala P, Chakravarthy AB, Gorge WJ, Knowland JG, Lattanze RK, Perrin SR, Scarantino CW, Townsend DW, Abramson RG, Yankeelov TE. Towards real-time topical detection and characterization of FDG dose infiltration prior to PET imaging. Eur J Nucl Med Mol Imaging. 2016;43:2374–2380.
16. Williams JM, Rani SD, Li X, Arlinghaus LR, Lee TC, MacDonald LR, Partridge SC, Kang H, Whisenant JG, Abramson RG, Linden HM, Kinahan PE, Yankeelov TE. Comparison of prone versus supine 18F-FDG-PET of locally advanced breast cancer: phantom and preliminary clinical studies. Med Phys. 2015;42:3801–3813.
17. Shankar LK, Hoffman JM, Bacharach S, Graham MM, Karp J, Lammertsma AA, Larson S, Mankoff DA, Siegel BA, Van den Abbeele A, Yap J, Sullivan D, National CI. Consensus recommendations for the use of 18F-FDG PET as an indicator of therapeutic response in patients in National Cancer Institute trials. J Nucl Med. 2006;47:1059–1066.
18. Delbeke D, Coleman RE, Guiberteau MJ, Brown ML, Royal HD, Siegel BA, Townsend DW, Berland LL, Parker JA, Hubner K, Stabin MG, Zubal G, Kachelriess M, Cronin V, Holbrook S. Procedure guideline for tumor imaging with 18F-FDG PET/CT 1.0. J Nucl Med. 2006;47:885–895.
19. OJ, Lodge MA, Wahl RL. Practical PERCIST: A Simplified Guide to PET Response Criteria in Solid Tumors 1.0. Radiology. 2016;280:576–584.
20. Altman DG, Bland JM. Measurement in medicine: the analysis of method comparison studies. Statistician. 1983;32:307–317.
21. Drisis S, El Adoui M, Flamen P, Benjelloun M, Dewind R, Paesmans M, Ignatiadis M, Bali M, Lemort M. Early prediction of neoadjuvant treatment outcome in locally advanced breast cancer using parametric response mapping and radial heterogeneity from breast MRI. J Magn Reson Imaging. 2019. [Epub ahead of print]
22. Eun NL, Kang D, Son EJ, Park JS, Youk JH, Kim JA, Gweon HM. Texture analysis with 3.0-T MRI for association of response to neoadjuvant chemotherapy in breast cancer. Radiology. 2020;294:31–41.
23. Golshan M, Wong SM, Loibl S, Huober JB, O'Shaughnessy J, Rugo HS, Wolmark N, AP, Maag D, Sullivan DM, Metzger-Filho O, V, Minckwitz G, Geyer CE, Jr., Sikov WM, Untch M. Early assessment with magnetic resonance imaging for prediction of pathologic response to neoadjuvant chemotherapy in triple-negative breast cancer: results from the phase III BrighTNess trial. Eur J Surg Oncol. 2020;46:223–228.
24. Partridge SC, Zhang Z, Newitt DC, Gibbs JE, Chenevert TL, Rosen MA, Bolan PJ, Marques HS, Romanoff J, Cimino L, Joe BN, Umphrey HR, Ojeda-Fournier H, Dogan B, Oh K, Abe H, Drukteinis JS, Esserman LJ, Hylton NM, Team AT, Investigators IST. Diffusion-weighted MRI findings predict pathologic response in neoadjuvant treatment of breast cancer: the ACRIN 6698 multicenter trial. Radiology. 2018;289:618–627.
25. Kang H, Hainline A, Arlinghaus LR, Elderidge S, Li X, Abramson VG, Chakravarthy AB, Abramson RG, Bingham B, Fakhoury K, Yankeelov TE. Combining multiparametric MRI with receptor information to optimize prediction of pathologic response to neoadjuvant therapy in breast cancer: preliminary results. J Med Imag. 2018;5:011015.
26. Li X, Abramson RG, Arlinghaus LR, Kang H, Chakravarthy AB, Abramson VG, Farley J, Mayer IA, Kelley MC, Meszoely IM, Means-Powell J, Grau AM, Sanders M, Yankeelov TE. Multiparametric magnetic resonance imaging for predicting pathological response after the first cycle of neoadjuvant chemotherapy in breast cancer. Invest Radiol. 2015;50:195–204.
27. Moy L, Noz ME, Maguire GQ, Jr., Melsaether A, Deans AE, Murphy-Walcott AD, Ponzo F. Role of fusion of prone FDG-PET and magnetic resonance imaging of the breasts in the evaluation of breast cancer. Breast J. 2010;16:369–376.
28. Pinker K, Bogner W, Baltzer P, Karanikas G, Magometschnigg H, Brader P, Gruber S, Bickel H, Dubsky P, Bago-Horvath Z, Bartsch R, Weber M, Trattnig S, Helbich TH. Improved differentiation of benign and malignant breast tumors with multiparametric 18fluorodeoxyglucose positron emission tomography magnetic resonance imaging: a feasibility study. Clin Cancer Res. 2014;20:3540–3549.
29. Schmitz J, Schwab J, Schwenck J, Chen Q, Quintanilla-Martinez L, Hahn M, Wietek B, Schwenzer N, Staebler A, Kohlhofer U, Aina OH, Hubbard NE, Reischl G, Borowsky AD, Brucker S, Nikolaou K, la Fougere C, Cardiff RD, Pichler BJ, Schmid AM. Decoding intratumoral heterogeneity of breast cancer by multiparametric in vivo imaging: a translational study. Cancer Res. 2016;76:5512–5522.